Tetrahedron 76 (2020) 131108

Contents lists available at ScienceDirect

Tetrahedron

journal homepage: www.elsevier.com/locate/tet

Novel 'naked-eye' Bis-Schiff base fluorescent chemosensors for sensitive detection of Zn^{2+} and bio-imaging in living cells

Xinchao Wang [a, **, 1], Ge Ding [b, *, 1], Yuanke Duan [a], Min Wang [a], Guangshi Zhu [a], Xiujuan Li [a, ***], Yanfen Zhang [a, ****], Xiaozhuan Qin [c, *****]

[a] College of Pharmacy, Heze University, Heze, Shandong Province, China
[b] Chongqing Key Laboratory of Environmental Materials & Remediation Technologies, College of Chemistry and Environmental Engineering, Chongqing University of Arts and Sciences, Yongchuan, 402160, China
[c] Zhengzhou Institute of Technology, School of Chemical Engineering & Food Science, Henan, Zhengzhou, 450044, China

ARTICLE INFO

Article history:
Received 5 January 2020
Received in revised form
4 March 2020
Accepted 6 March 2020
Available online 17 March 2020

Keywords:
ESIPT
Organic chromophore
Zinc ion sensors
Naked-eye emission
Cell imaging

ABSTRACT

Novel chemosensors based on excited state intramolecular proton transfer chemosensors (F1, F3, F5) and reference dyes (F2, F4, F6) are presented in this work. Target dyes F1, F3 and F5 display high selectivity and sensitivity toward Zn^{2+} in solvents (such as EtOH, EtOH/PBS buffer) in the presence of competitive ions (K+, Na+, Ni2+, Pb2+, Mn2+, Mg2+, Hg2+, Cu2+,Cd2+, Cr3+, Fe3+). Sensing property for Zn^{2+} was studied by UV–Visible, fluorescence spectrophotometric analyses and Job's plot analyses. F1, F3 and F5 for Zn^{2+} detection revealed extremely low detection limit (67.2 nM), high anti-interference ability, and the immediate response. Furthermore, inverted fluorescence microscopy imaging experiment were also investigated, the results demonstrated that the probes have well cell membrane permeability and hypotoxicity. Simultaneously, due to the ability to adapt a wider range of pH, the probes could also image Zn^{2+} in live cells with remarkable fluorescence variation and provide a new method to visualize monitoring in live cells.

© 2020 Elsevier Ltd. All rights reserved.

1. Introduction

In the last two decades, fluorescent probes or chemosensors for selective recognition of metal ions have drawn considerable interests due to its great application potentials in a variety of fields including analytical chemistry, medicine, biology, environment processes and so on, which is based on various superior advantages of possessing high sensitivity, selectivity, simplicity and instantaneous response [1–5]. Zn^{2+} is one of the important trace elements in living organisms, and it is widely distributed in living organisms [6]. It plays a vital role in physiological processes such as enzyme catalysis [7], protein sequencing [8], and gene expression [9]. Simultaneously, Zinc deficiency is one of the main causes of genetic defects in children's growth period [10]. Hence, it is one of our main concerns to development of artificial chemosensors for recognition of Zn^{2+} ion in environmental as well as biological samples.

Recently, several zinc sensors have been developed based on different fluorophores such as quinoline [11], fluorescein [12], coumarin [13] and pyrene [14]. Fluorophores with excited state intramolecular proton transfer (ESIPT) properties are a kind of substance with good biological activity, such as the complex formed by Schiff base and metal ion exhibits good biological activity in bacteriostatic, bactericidal, antitumor and fluorescence detection [15–18]. Photophysical properties of excited state intramolecular proton transfer (ESIPT) processes in fluorescence spectroscopy have generated considerable interest for both fundamental investigations and applications of organic molecules [19–23]. Therefore, the improvement or inhibition of the ESIPT process may have a significant effect on the normal fluorescence emission peak, especially the Schiff base containing a trifluoromethylaryl group, which is widely used in the fields of bioluminescence detection and medical analysis. Organic molecules exhibiting ESIPT properties are one of the powerful potential

* Corresponding author.
** Corresponding author.
*** Corresponding author.
**** Corresponding author.
***** Corresponding author.
E-mail addresses: wxc198566@126.com (X. Wang), dingge1989cqu@126.com (G. Ding), 1103361352@qq.com (Y. Duan).
[1] Xinchao Wang and Ge Ding are designated as the co-first authors, who make equal contribution to this study.

https://doi.org/10.1016/j.tet.2020.131108
0040-4020/© 2020 Elsevier Ltd. All rights reserved.

candidates as the fluorescent chemosensors due to the sensitive decay in the excited singlet states, and ESIPT fluorophores have an unusually large Stokes shift (~200 nm) when compared to traditional fluorophores (fluorescein, rhodamine, etc.). This helps avoid unwanted self-reabsorption and inner-filter effects. Furthermore, ESIPT compounds including N, O and S donor atoms are within the oldest ligands in coordination chemistry, and they can form stable complexes with some metal ions easily [24]. While so far, most ESIPT chemosensors are limited to benzotriazole derivatives [25–27], and very few ESIPT chemosensors contains trifluoromethyl have been reported up to date [28,29]. Furthermore, for Zn^{2+} sensors, most of them have the drawback of inadequate selectivity towards Zn^{2+} due to special interference [30].

Taking into account concerns mentioned above, a series new bis-Schiff base fluorescent chemosensors (F1/F3/F5 as the target dyes and F2/F4/F6 as the reference dyes shown in Scheme 1) contains trifluoromethyl groups and different ether backbone are designed and synthesized, in which the pendant group -OH and-C═N act as the recognition moiety.

It is demonstrated that the target compounds with ESIPT properties show good photochromic properties and exhibit "naked-eye" recognition and a notable fluorescence "turn-on" in the presence of Zn2+ with high selectivity and sensitivity in many solvents (such as Ethanol、Ethanol/PBS buffer, DMF、ACN). In contrast, the reference dyes (F2/F4/F6) lack of -OH group only show normal emission properties. Furthermore, fluorescence imaging for Zn2+ in living SW620 cells proves its value of potential application in biological systems.

2. Results and discussions

The UV–Vis absorption spectra and fluorescence spectra of the target and reference molecules in various solvents are determined. The typical absorption spectra of F3 and F4 in pure ethanol are shown in Fig. 1 (a). The UV spectra show that F3 and F4 display a little difference in spectral shape, while the absorption wavelength maximum of F3 exhibits a red shift (22 nm, F3, 346 nm, F4, 324 nm) comparing with F4. Furthermore, the absorbance intensity of F4 is higher than that of F3 at range of 250–340 nm (also see Tables S1 and SI). Those phenomena shows that the red-shift in the absorption maximum of F3 with respect to that of F4 is attributed to the presence of intramolecular H-bonding effect between O–H and CH═N groups and increase in molecular conjugation in F3, the maximum absorption wavelength of the target dyes increase gradually (F3>F1> F5) due to the increase in conjugation, and the partners F1/F2 and F5/F6 also show the similar absorption spectral properties as F3/F4 (typically shown in Fig. S1, also see Tables S1 and SI).

The different emission spectra between the target and the reference dyes are presented in Fig. 1 (b). The target dyes F1/F3/F5 present well-separated dual emission peaks in various organic solvents including the first emission band peaked around 400 nm with the normal Stokes shift (approximate 50 nm in ethanol, typically depicted in Fig. 1 (b)), and the second emission band presents obvious red shift comparing to the first emission band (such as F1, 169 nm, F3, 171 nm, in ethanol). By contrast, reference dyes F2, F4 and F6 show only a single emission band peaked at 400 nm. The results suggest that the first emission bands of the fluorescent chemosensors are ascribed to the normal enol emission decay, while the second emission bands of F3 could be assigned to keto tautomer produced by intramolecular proton transfer in the excited state (ESIPT) through a representative four-level cycle photo-process (Scheme S1, SI). The partners F1/F2 and F5/F6 also show the similar fluorescence spectral properties as F3/F4 (typically shown in Fig. S2, also see Tables S1 and SI).

Spectral properties of the target molecules induced by various metal ions in ethanol are measured at room temperature (Fig. 2, Fig. S3 & Fig. S4, SI). Take F3 and the reference F4 as example, Fig. 2 (a/b) shows the UV–Vis absorption spectra and fluorescence spectra of F3 respectively upon addition Zn2+ (C = 1 × 10-7 mol.L−1) and various other metal ions (including K+, Na+, Ni2+, Pb2+, Mn2+, Mg2+, Hg2+, Cu2+,Cd2+, Cr3+, Fe3+, C = 1 × 10-6 mol.L−1). It could be clearly seen that none of these metal ions led to significant enhancement in the fluorescence intensity or obviously changes in the UV–Vis absorption spectrum of F3 except for Zn2+, which result in a more than 40 folds (F3, 0.0032, in EtOH; 0.128, after Zn2+ addition) fluorescence enhancement and a shoulder peaked at 410 nm of absorption spectrum. It must be pointed out that with the addition of Zn2+, the ESIPT peak at 530 nm disappears in ethanol, and a new peak with significant fluorescence enhancement appears at 500 nm, which may be due to the chelation of Zn2+ with the target compound F3 and restrict C═N isomerization mechanism. Comparing to other target dyes, it also results in a almost 35 folds (F1, 0.0030, in EtOH; 0.105; F5, 0.0028, in EtOH; 0.1008, after Zn2+ addition) fluorescence enhancement and a shoulder peaked at 408 nm of absorption

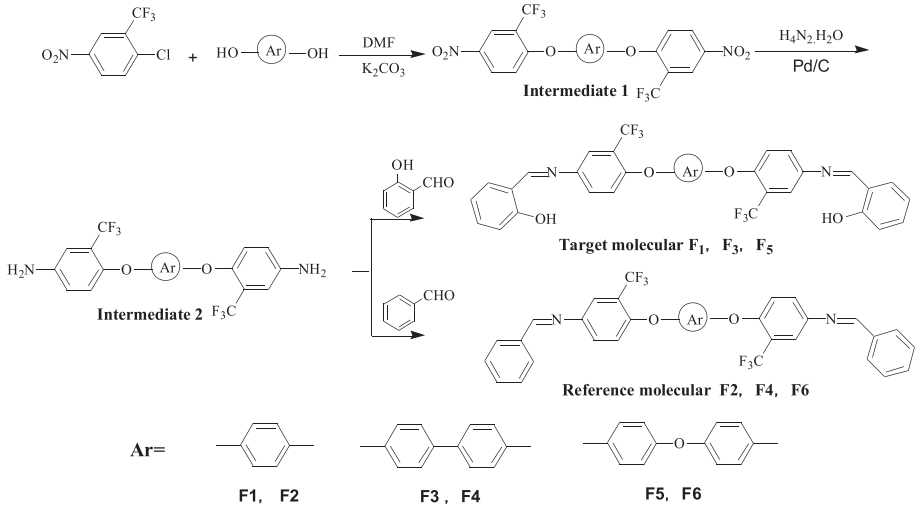

Scheme 1. Chemical structures of the molecules studied in this work.

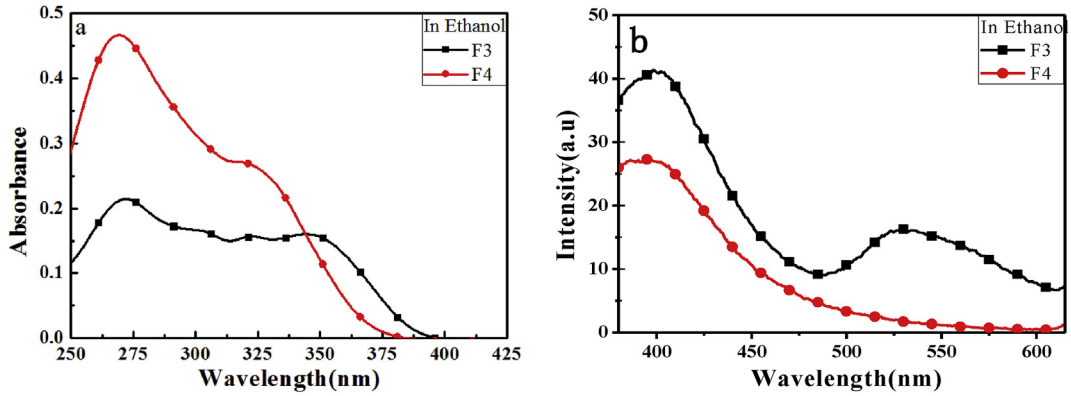

Fig. 1. UV–Vis absorbance spectrum (a) and fluorescence emission spectrum (b) of F3 and F4 in ethanol ($C = 5.0 \times 10^{-6}$ mol. L^{-1}), excitation wavelength, 320 nm.

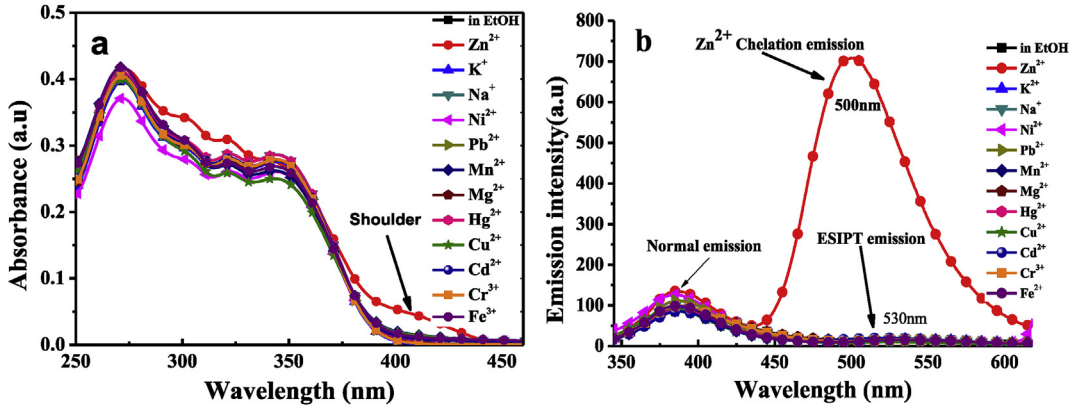

Fig. 2. (a) UV–Vis absorption spectrum and (b) Fluorescence emission spectrum changes of F3 induced by different metal ions in Ethanol ($C_{F3} = 5.0 \times 10^{-6}$ mol. L^{-1}, $C_{Ions} = 1.0 \times 10^{-7}$ mol. L^{-1}), excitation wavelength, 320 nm.

spectrum, which means that the bigger in molecular conjugation the better in zinc recognition. At the same time, the spectral properties of the reference molecule F4, F2 and F6 show no any significant change in the addition of the above ions (Figure S5 & Figure S6, SI). It is worth mentioning that the similar phenomenon is also found in other organic solution (such as DMSO, CAN, Ethanol/PBS buffer). Hence, it could be considered that the chelation of Zn2+ ions does greatly suppress the occurrence of ESIPT.

In addition to the interference experiment in the presence of different ions, we also analyzed whether the different pH value had an effect on the identification of zinc ions for sensors. Take prober F3 for example (Figure S7, SI), it could be seen clearly that UV–Vis spectrum of F3 almost kept the same as in neutral environment when zinc ions was added under the different pH environment (value of pH from 2.0 to 10.0), this result proved an evidence that a wide range of pH changes has no obvious effect on the basic characteristics of probe sensing. Thus, this phenomenon opens up the possibility for zinc ions detection in living cell or cell imaging.

It is acceptable that the Zn2+ ion has four sp3 hybrid orbitals with a regular coordination tetrahedral geometry [31]. The target probe molecule F3 has -C═N、-OH groups which containing lone pairs of electrons can chelate with Zn2+ to form a conjugated large Pi bond, thereby the fluorescence intensity has a remarkable enhancement. Other ions, such as Hg2+ ions, are characterized by three coordinated sp2 hybrid orbitals with flat triangular chelation geometry, so that the target compound cannot be effectively complexed with Hg2+. It is worth noting that the target molecule has a bis-Schiff base structure, so Zn2+ could coordinated with C═N and -OH groups (Scheme 2) [32–34].

Chemical shifts of probe were identified by the 1H-NMR titration analysis through addition Zn2+ and without Zn2+ (Fig. 3). When probe F3 was added different concentration of Zn2+ ions gradually (from 0 to 1.0 equiv.), the hydroxyl peak at 12.874 ppm gradually decreased and totally disappeared on addition of 1.0 equiv. of Zn2+. Furthermore, small downfield shifts were found in the aromatic region. These shifts clearly indicated that the F3-Zn2+ complex were formed successfully.

In order to further determine the higher selectivity of target dyes to zinc ion, the competition experiments were also carried out by monitoring the change in fluorescence emission intensity at 500 nm upon addition of Zn^{2+} (1×10^{-7} mol. L^{-1}) and different metal ions (5×10^{-6} mol. L^{-1}) to a solution of target dyes in ethanol solution, Zn^{2+} could be recognized obviously through a dramatically fluorescence emission enhancement in ethanol aqueous solution, which could be observed distinctly through “naked-eye” color change from colorless to bluish green due to OFF-ON process under the UV lamp (typically shown in Fig. 4 (a)). It could be seen that a slight or negligible variation could be observed as the addition of other metal ions aqueous solutions. At the same time, as the conjugation extent of the target molecules (F3>F1>F5) increase, the fluorescence emission intensity increases accordingly (also see in Figure S8, SI). However, the reference molecules do not show any significant changes under the UV lamp (Figure S9, SI). Further investigation shows that the presence of the other interfered ions does not exhibit remarkable influence on the sensing response of the substrates to Zn^{2+} in ethanol aqueous solution, which are

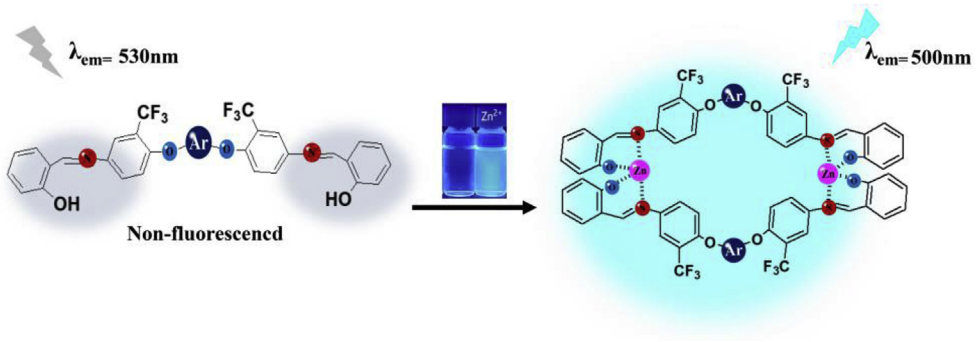

Scheme 2. Fluorescence emission variation of F3 induced by Zn^{2+} addition and the proposed binding mode.

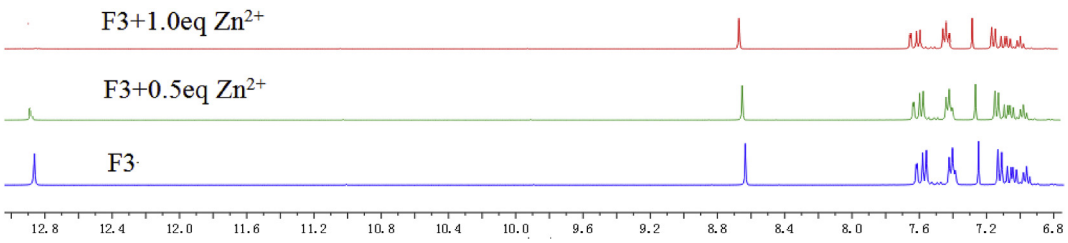

Fig. 3. ^{1}H-NMR spectra of F3 and F3-Zn^{2+}.

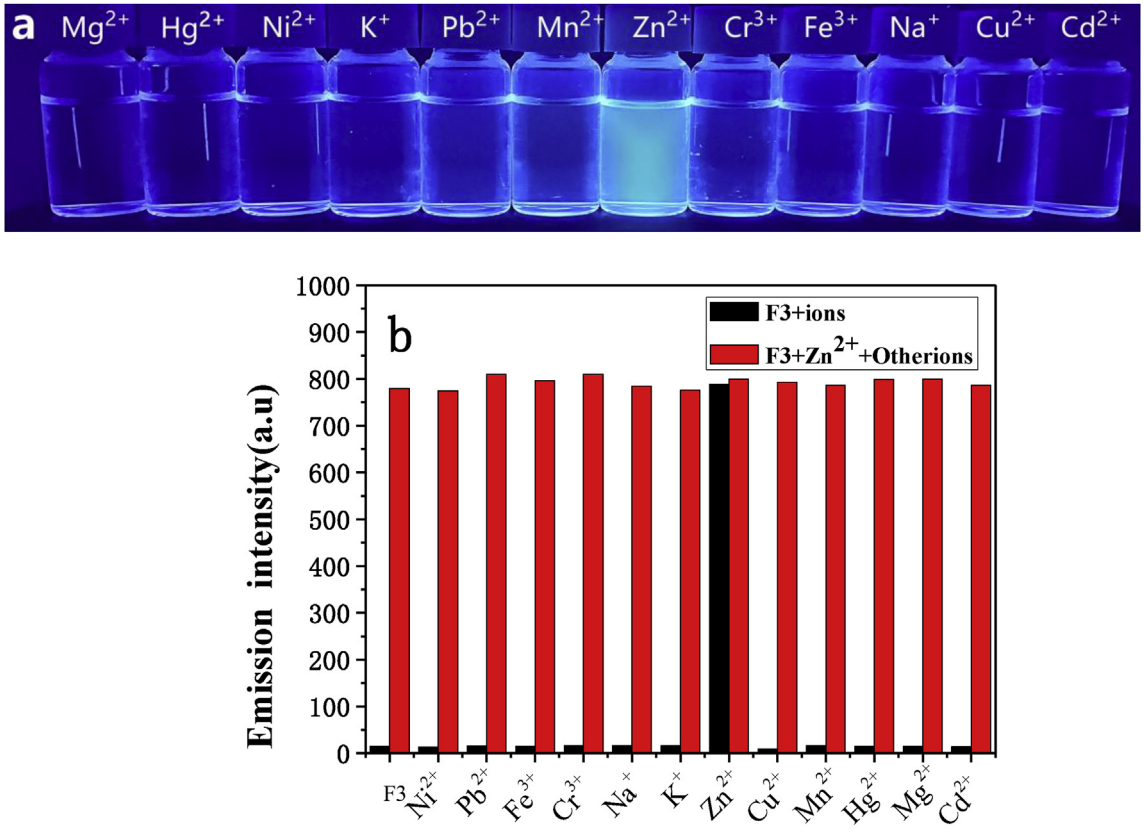

Fig. 4. (a) Fluorescence emission intensity changes of F3 induced by different metal ions in ethanol under UV lamp. (b) Metal ions competition analysis of F3 (5×10^{-6} mol. L^{-1}) in EtOH. The black bars represent fluorescence emission of F3 after addition of other metal ions (1×10^{-7} mol. L^{-1}). The red bars represent fluorescence changes that occur upon addition of 1×10^{-7} mol. L^{-1} of other metal ions to solution containing F3 and Zn^{2+} (1×10^{-7} mol. L^{-1}).

shown in Fig. 4 (b) and Fig. S10 (SI). These results further indicate that the target fluorescent probes can strongly coordinate with Zn^{2+} and restricted the occurrence of C=N isomerization, which blocks ESIPT reaction.

We further detected the fluorescence intensity of probes with Zn^{2+} in different volume ratio of PBS/EtOH (from 0: 10 to 10: 0, v/v, pH = 7.20) system and the fluorescence titration curve of target dyes with Zn2+(Fig. 5, Fig. S11 & Fig. S12, SI) in pure ethanol and in ethanol/PBS buffer (1/1, v/v, pH = 7.20) mixed solution, respectively, take F3 for example. It can be clearly seen that the emission peak generated by Zn2+ chelation at 500 nm with a sharp enhancement in peak intensity as Zn2+ was gradually added (1.0 × 10-7 mol. L−1 to 1.0 × 10-4 mol. L−1), and further increasing the amount of Zn2+ only led to small changes in the fluorescence intensity. Simultaneously, Fig. 5 and Fig. S11 & Fig. S12 (SI) indicated that the fluorescence titration curve in pure ethanol and in ethanol/buffer mixed solution all displayed the almost similar emission variation. Meanwhile, as the PBS volume increased, the formed Zn2+ complex can still maintain a strong fluorescence emission.

The coordination constant was determined by the measurement of the fluorescence spectra changes according to Benesi-Hildebrand equation. The equation is described as followings:

$$F_0 \Big/ (F_0 - F) = F_0 \Big/ (F_0 - F_{complex}) + F_0 \Big/ (F_0 - F_{complex}) \times 1 \Big/ K \times 1 \Big/ [M] \quad (1)$$

wherein K represents the binding constant, F0 is the integrated fluorescence intensity of free ligand, F shows the observed integrated fluorescence intensities, Fcomplex is the emission intensities of the ligand-metal complex, and [M] shows the concentration of Zn ions. The binding constant is given by the ratio intercept/slope from the plot of F0/F0-F versus 1/[*M*]. The curve fitting of the fluorescence intensity of F3 to the reciprocal of the Zn2+ concentration further demonstrates the linear characteristics of complex (Fig. 6). From the fluorescence titration data, sensor F3 for the detection of Zn^{2+} revealed extremely low detection limit (67.2 nM), the binding constants (Ka) of the probe-Zn^{2+} complex were determined as 1.37 × 106 L/mol (F1), 1.42 × 106 L/mol (F3) and 1.13 × 106 L/mol (F5), respectively (Fig. S13, SI). The larger binding constant (Ka) means probe-Zn^{2+}complex possesses much more stabilities.

Job's plot analysis of the fluorescence data was shown that the stoichiometric ratio was 1: 1 for the probes (F1/F3/F5)-Zn^{2+} complex (see Scheme 2, Fig. 7 & Fig. S14,SI). The fluorescence titration test of probe under the existence of different Zn^{2+} concentrations was performed in EtOH solution. Keeping the total concentration of the probe and Zn^{2+} for 5.0×10^{-6} mol/L, and the concentration ratio of 1:9, 2:8, 3:7, 4:6, 5:5, 6:4, 7:3, 8:2 and 9:1 between probe and Zn^{2+} was titrated.

To ensure F3 could be used for detecting Zn^{2+} in living cells, toxicity assay was also performed by adding a series of concentrations (0, 2, 4, 25, 50, 100 μM) of probe F3 in living human colonic cancer cells line (SW620), the cells survival rate higher than 96% in every concentration gradient, which indicates that probe F3 has no apparent toxicity to living SW620 cells. The hypotoxicity of probe F3 clearly demonstrates that probe has low cytotoxicity to living cells.

To further explore the potential biological application, the probe was applied in SW620 cancer cells by fluorescence imaging experiment shown in Fig. 8. Firstly, SW620 cells incubation with 1% DMSO-containing F3 for 0.5 h at 37 °C, and no obviously fluorescence can be observed under the fluorescence microscope (Fig. 8 (b)). However, the green fluorescence was observed under the

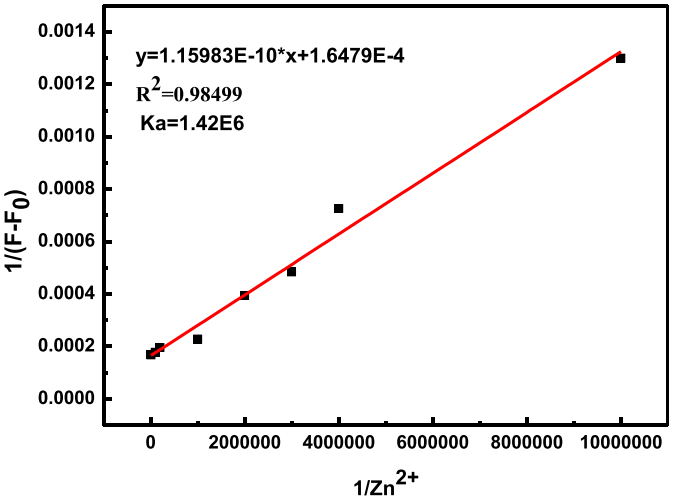

Fig. 6. Fluorescence emission spectra of F3 ($C_{F3} = 5.0 \times 10^{-6}$ mol. L^{-1}) upon the titration of Zn^{2+} ($C_{Ions} = 0–1.0 \times 10^{-4}$ mol. L^{-1}) in EtOH solution.

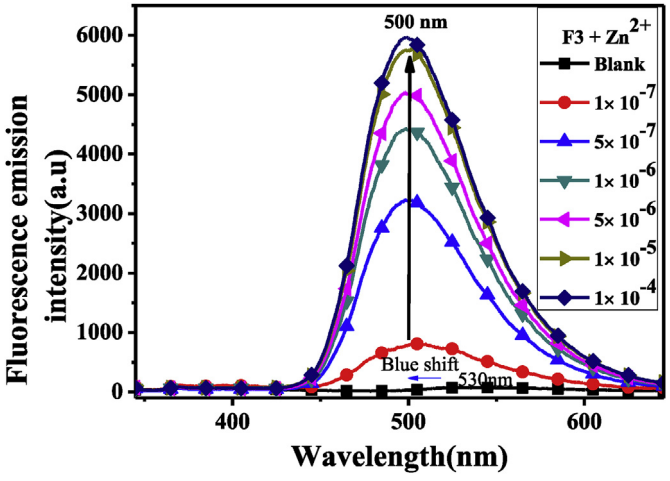

Fig. 5. Fluorescence spectra of ligand F3 measured in ethanol upon addition Zn^{2+} and after the addition of increasing amounts of Zn^{2+} ($C_{F3} = 5.0 \times 10^{-6}$ mol. L^{-1}, $C_{Ions} = 0–1.0 \times 10^{-4}$ mol. L^{-1}).

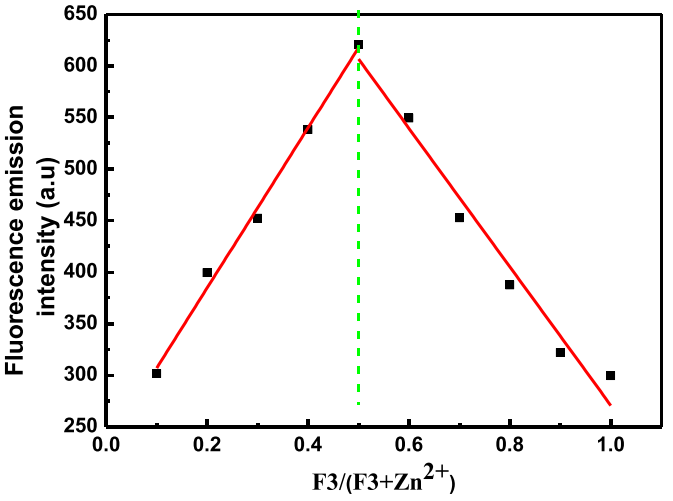

Fig. 7. Job's plot for F3 with Zn^{2+} ions in EtOH solution.

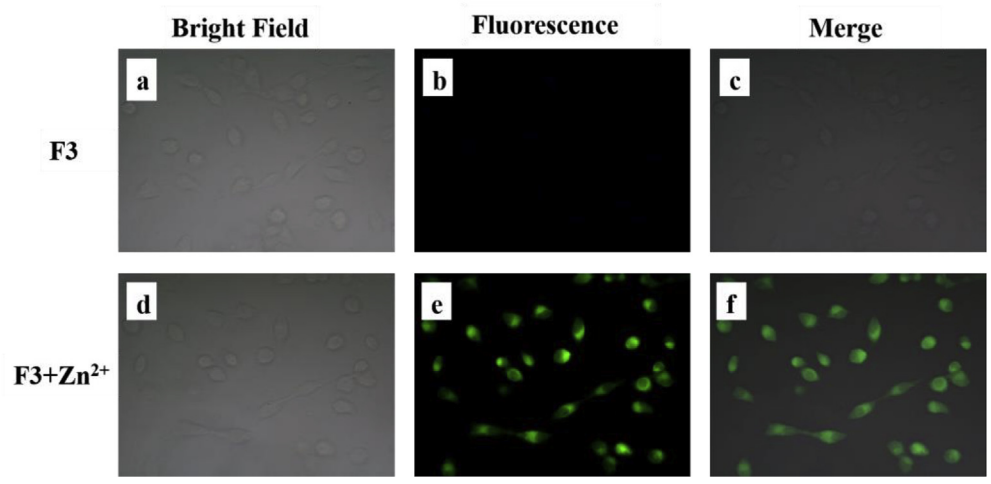

Fig. 8. Confocal fluorescence images of SW620 cells. (a–c) Cells cultured with F3 (1×10^{-6} mol.L^{-1}) for 0.5 h; (d–f) Cells treated with F3 (1×10^{-6} mol.L^{-1}) and then incubated with 5×10^{-6} mol.L^{-1} Zn^{2+} ions for another 0.5 h. Excitation wavelength, 320 nm, emission wavelength, 500 nm.

fluorescence microscope after incubation of the probe F3 treated cells with Zn^{2+} for another 0.5 h at the same conditions (Fig. 8 (e)). The experiments indicated F3 could be served as an efficient candidate for monitoring changes in the intracellular Zn^{2+} under biological conditions.

3. Experimental section

3.1. Material and characterization

The organic solvents were purchased by the Sigma-Aldrich Corporation and were further processed by the standard laboratory method. The starting materials for the preparation of new studied chemosensors in our own laboratory were supplied by the Acros Corporation.

The ^{1}H and ^{13}C nuclear magnetic resonance (NMR) spectra of the studied dyes molecules were measured by the Bruker apparatus (400 MHz) in standard NMR tubes at the room temperature. The ^{1}H and ^{13}C NMR peak chemical shifts of the target molecules were calculated by an internal reference tetramethylsilane (TMS). A Beijing Fukai melting point apparatus was employed to determine the melting points of the samples. The elemental analysis of the prepared dye molecules was acquired by a CE440 elemental analysis meter from Exeter Analytical Inc.

3.2. UV/visible absorption spectral determination and fluorescence emission spectral measurement

The UV/visible absorption spectra and fluorescence emission spectra of the samples were surveyed by using the spectral grade solvents. A TU1901 spectrophotometer from Beijing PUXI General Equipment Limited Corporation was employed to determine the UV/visible absorption spectra of the samples. The spectrofluorophotonmeter (Cary eclipse) was used to determine the fluorescence emission spectra of the samples. The fluorescence quantum yields of the organic dyes in the solvents were measured by using quinine sulfate in 0.5 mol/L H_2SO_4 (Φ, 0.546) as reference [35].

3.3. Synthesis of the studied target dyes

The synthesis routes of the new studied dyes F1-F6 were presented in Scheme 1. The preparation details of these target dyes, molecular structural characterization of the intermediates and the final molecules were described in “supporting information (SI)”.

3.4. The determination of DL

The detection limit (DL) was determined according to formula (2) by emission data of probes upon gradual addition of Zn^{2+}.

$$DL = 3\delta/S \quad (2)$$

where δ was the standard deviation of blank ample, S represented the absolute value of the slope between fluorescence intensity and Zn^{2+} concentration.

3.5. Bioimaging experiment

SW620 cells were cultured in DMEM (containing 10% FBS) in a humidified incubator at 37 °C and 5% CO_2. The cells were seeded 2.5×10^{5} per well in six-well plates. After 18 h proliferation, the compound F3 at the final concentration of 1×10^{-6} mol/L (containing 1% DMSO) were exposed to the cells and incubated for an additional 30 min at 37 °C. Then, the medium was discarded, and the cells were washed once with phosphate buffer saline (PBS). After that, the Zn^{2+} solution was added to the wells with a final concentration of 5×10^{-6} mol/L, and the cells were incubated at 37 °C for another 0.5 h. The cells were washed with cold PBS for three times and fixed with 4% of paraformaldehyde PBS solution at 4 °C for 15 min, then PBS was used to rinse cells for three times. Finally, the cells were observed with a confocal microscope.

4. Conclusions

In conclusion, a series of novel ‘naked-eye’ Bis-Schiff base fluorescent chemosensors are successfully synthesized. The results of ultraviolet visible absorption spectra and fluorescent emission spectra indicate that the target compounds have a unique selectivity and highly sensitivity for the ‘naked-eye’ detection of Zn^{2+}, and the bigger in molecular conjugation the better in zinc recognition. Furthermore, for the good acid-base adaptation, the bioimaging experiment has successfully conducted as a fluorescent probe to detect the Zn^{2+} in SW620 cells. This work provides a useful design strategy for constructing fluorescent sensors for the recognition of specific metal ions by rational structural design.

Declaration of competing interest

The authors declare no competing financial interest.

Acknowledgements

We thank warm encouragement of the HeZe University PhD Fund Planning (No.XY16BS33), Heze University Scientific Research Foundation (No.XY17KJ10,NO.XY18PY02,NO.XY18PY08). G.D. thanks a lot for the financial support of Chongqing Science and Technology Commission (NO. cstc2018jcyjAX0446) and Chongqing University of Arts and Sciences Scientific Research Foundation (NO. 2017RCH03) and X.Q. thanks the financial support of the Department of Science and Technology of Henan province (No. 192102210201).

Appendix A. Supplementary data

Supplementary data to this article can be found online at https://doi.org/10.1016/j.tet.2020.131108.

References

[1] G. Kasirajan, V. Krishnaswamy, R. Nandhakumar, M. Mahalingam, M. Sadasivam, M.P. Subramaniam, S. Ramasamy, New pyrazolo-quinoline scaffold as a reversible colorimetric fluorescent probe for selective detection of Zn^{2+} ions and its imaging in live cells, J. Photochem. Photobiol. Chem. 341 (2017) 136–145.

[2] G. Zhao, B.Y. Guo, G. Wei, S.Y. Guang, Z.Y. Gu, H.Y. Xu, A novel dual-channel Schiff base fluorescent chemo-sensor for Zn^{2+} and Ca^{2+} recognition: synthesis, mechanism and application, Dyes Pigments 170 (2019) 107614.

[3] F. Wang, J.H. Moon, R. Nandhakumar, B. Kang, D. Kim, K.M. Kim, J.Y. Lee, J. Yoon, Zn^{2+}-induced conformational changes in a binaphthyl-pyrene derivative monitored by using fluorescence and CD spectroscopy, Chem. Commun. 49 (2013) 7228–7230.

[4] Z. Kowser, U. Rayhan, S. Rahman, P.E. Georghiou, T. Yamato, A fluorescence "turn-on" sensor for multiple analytes: OAc^- and F^- triggered fluorogenic detection of Zn^{2+} in a co-operative fashion, Tetrahedron 73 (2017) 5418–5424.

[5] C.R. Li, S.L. Li, Z.Y. Yang, Development of a coumarin-furan conjugate as Zn^{2+} ratiometric fluorescent probe in ethanol-water system, Spectrochim. Acta Mol. Biomol. Spectrosc. 174 (2017) 214–222.

[6] E.L. Que, D.W. Domaille, C.J. Chang, Metals in neurobiology: probing their chemistry and biology with molecular imaging, Chem. Rev. 108 (2008) 1517–1549.

[7] J.H. Viles, Metal ions and amyloid fiber formation in neurodegenerative diseases. Copper, zinc and iron in Alzheimer's, Parkinson's and prion diseases, Coord. Chem. Rev. 256 (2012) 2271–2284.

[8] T. Jiang, X. Xiong, S.Y. Luo, Q. Fei, A. Yu, Z. Zhu, Direct mass spectrometric analysis of zinc and cadmium in water by microwave plasma torch coupled with a linear ion trap mass spectrometer, Int. J. Mass Spectrom. 399 (2016) 33–39.

[9] N. Pourhassanali, S. Roshan-Milani, F. Kheradmand, M. Motazakker, M. Bagheri, E. Saboory, Zinc attenuates ethanol-induced Sertoli cell toxicity and apoptosis through caspase-3 mediated pathways, Reprod. Toxicol. 61 (2016) 97–103.

[10] D.G. Alison, J.S. Kerry, P.S. Christine, P.W.J. Keith, C. Parul, Micronutrient deficiencies in pregnancy worldwide: health effects and prevention, Nat. Rev. Endocrinol. 12 (2016) 274–289.

[11] K.S. Hwa, Y.O. Seung, P. Chulhwan, K. Young, Colorimetric detection of Co2+ ion using silver nanoparticles with spherical, plate, and rod shapes, Langmuir 29 (2013) 8978–8982.

[12] Y.C. Chen, C.C. Zhu, J.J. Cen, Y. Bai, W.J. He, Z.J. Guo, Ratiometric detection of pH fluctuation in mitochondria with a new fluorescein/cyanine hybrid sensor, Chem. Sci. 6 (2015) 3187–3194.

[13] D. Maity, T. Govindaraju, A differentially selective sensor with fluorescence turn-on response to Zn^{2+} and dual-mode ratiometric response to Al^{3+} in aqueous media, Chem. Commun. 48 (2012) 1039–1041.

[14] Y. Yang, C. Ma, Y. Zhang, Q. Xue, H. Guo, A highly selective "turn-on" fluorescent sensor for zinc ion based on a cinnamyl pyrazoline derivative and its imaging in live cells, Anal. Methods 16 (2018) 1833–1841.

[15] A.C. Sedgwick, L.L. Wu, H.H. Han, S.D. Bull, X.P. He, T.D. James, J.L. Sessler, B.Z. Tang, H. Tian, J.Y. Yoon, Excited-state intramolecular proton-transfer (ESIPT) based fluorescence sensors and imaging agents, Chem. Soc. Rev. 47 (2018) 8842–8880.

[16] J. Massue, D. Jacquemin, G. Ulrich, Molecular engineering of excited-state intramolecular proton transfer (ESIPT) dual and triple emitters, Chem. Lett. 47 (2018) 1083–1089.

[17] L.L. Wu, Y. Wang, M. Weber, L.Y. Liu, A.C. Sedgwick, S.D. Bull, C.S. Huang, T.D. James, ESIPT-based ratiometric fluorescence probe for the intracellular imaging of peroxynitrite, Chem. Commun. 71 (2018) 9953–9956.

[18] X.C. Wang, H.Y. Ma, G. Ding, Y. Lu, Y.L. Gong, S.T. Zhang, Z.P. Luo, H.R. Li, F. Gao, New armed near-IR two-photon organic chemosensors undergoing ESIPT and'naked eye'fluorescence sensing to zinc ions, Tetrahedron Lett. 56 (2015) 2758–2763.

[19] S. Sinha, B. Chowdhury, P.A. Ghosh, Highly sensitive ESIPT-based ratiometric fluorescence sensor for selective detection of Al^{3+}, Inorg. Chem. 55 (2016) 9212–9220.

[20] L. Chen, D. Wu, J.M. Kim, J. Yoon, An ESIPT-based fluorescence probe for colorimetric, ratiometric, and selective detection of phosgene in solutions and the gas phase, Anal. Chem. 89 (2017) 12596–12601.

[21] I.J. Chang, K.S. Hwang, S.K. Chang, Selective Hg^{2+} signaling via dithiane to aldehyde conversion of an ESIPT fluorophore, Dyes Pigments 137 (2017) 69–74.

[22] J. Zhou, R. Shi, J. Liu, R. Wang, Y. Xu, X. Qian, An ESIPT-based fluorescent probe for sensitive detection of hydrazine in aqueous solution, Org. Biomol. Chem. 13 (2015) 5344–5348.

[23] Y. Deng, X.Y. Min, L.L. Liu, R. Zhong, X. Xiao, J.M. Luo, X.B. Luo, New insight on the adsorption capacity of metallogels for antimonite and antimonate removal: from experimental to theoretical study, J. Hazard Mater. 36 (2018) 218–225.

[24] I. Nemec, R. Boca, M. Gembicky, L. Dlhan, R. Herchel, F. Renz, High-spin Schiff-base dinuclear iron (III) complexes bridged by N-oxide ligands, Inorg. Chim. Acta. 362 (2009) 4754–4759.

[25] Y. Xu, L. Xiao, S. Sun, Z. Pei, Y. Pei, Y. Pang, Switchable and selective detection of Zn^{2+} or Cd^{2+} in living cells based on 3'-o-substitutedarrangement of benzoxazole-derived fluorescent probes, Chem. Commun. 50 (2014) 7514–7516.

[26] A. Mahapatra, P. Karmakar, S. Manna, K. Maiti, D. Mandal, Benzthiazole-derived chromogenic, fluorogenic and ratiometric probes for detection of hydrazine in environmental samples and living cells, J. Photochem. Photobiol. Chem. 334 (2017) 1–12.

[27] Y. Gong, Z. Wang, S. Zhang, Z. Luo, F. Gao, H. Li, New ESIPT-inspired photostabilizers of two-photon absorption coumarin-benzotriazole dyads: from experiments to molecular modeling, Ind. Eng. Chem. Res. 55 (2016) 5223–5230.

[28] S.N. Yu, Z.C. Li, Y.Z. Hu, D.X. Yin, Synthesis of bis-schiff base compound with trifluoromethyl, Chin. J. Synth. Chem. 2 (2010) 226–228.

[29] A. Maliakal, G. Lem, N.J. Turro, R. Ravichandran, J.C. Suhadolnik, A.D. DeBellis, M.G. Wood, J. Lau, Twisted intramolecular charge transfer states in 2-arylbenzotriazoles: fluorescence deactivation via intramolecular electron transfer rather than proton transfer, J. Phys. Chem. A. 106 (2002) 7680–7689.

[30] A.O. Eseola, H. Görls, M. Bangesh, W. Plass, ESIPT-capable 2,6-di (1*H*-imidazol-2-yl) phenols with very strong fluorescent sensing signals towards Cr (iii), Zn (ii), and Cd (ii): molecular variation effects on turn-on efficiency, New J. Chem. 42 (2018) 7884–7900.

[31] A.B. Davis, A Library of Coumarin-Enaminone Chemodosimeters for the Detection of Analytes, Dissertations, 2016, p. 402.

[32] R. Chandra, A.K. Manna, M. Sahu, K. Rout, G.K. Patra, Simple salicylaldimine-functionalized dipodal *bis* Schiff base chromogenic and fluorogenic chemosensors for selective and sensitive detection of Al^{3+} and Cr^{3+}, Inorg. Chim. Acta. 499 (2019) 119192.

[33] S. Mondal, S.M. Mandal, D. Ojha, D. Chattopadhyay, C. Sinha, Water soluble sulfaguanidine based Schiff base as a "Turn-on" fluorescent probe for intracellular recognition of Zn^{2+} in living cells and exploration for biological activities, Polyhedron 172 (2019) 28–38.

[34] V. Venkatesan, K.R. Selva, S.K.A. Kumar, S.K. Sahoo, Highly selective turn-on fluorogenic chemosensor for Zn^{2+} based on chelation enhanced fluorescence, Inorg. Chem. Commun. 102 (2019) 171–179.

[35] L. Ilies, Y. Sato, C. Mitsui, H. Tsuji, E. Nakamura, Modular synthesis of polybenzo, [*b*]silole compounds for hole-blocking material in phosphorescent organic light emitting diodes, Chem. Asian J. 5 (2010) 1376–1381.